Charge Carrier Dynamics in Alternating Polyfluorene Copolymer:Fullerene Blends Probed by Terahertz Spectroscopy

Hynek Němec,*,† Han-Kwang Nienhuys,‡ Fengling Zhang,§ Olle Inganäs,§ Arkady Yartsev,† and Villy Sundström†

Department of Chemical Physics, Lund University, Getingevägen 60, 222 41 Lund, Sweden, Institute for Atomic and Molecular Physics, Kruislaan 407, 1098SJ Amsterdam, Netherlands, and Biomolecular and organic electronics, IFM, Linköping University, 581 53 Linköping, Sweden

Received: October 20, 2007; In Final Form: February 18, 2008

Time-resolved terahertz spectroscopy is used for investigation of photoinduced charge carrier dynamics in blends of a polyfluorene copolymer (poly[2,7-(9,9-dioctyl-fluorene)-alt-5,5-(4′,7′-di-2-thienyl -2′,1′,3-benzothiadiazole)]) and an electron acceptor ([6,6]-phenyl-C_{61}-butyric acid methyl ester). The transient far-infrared response appears instantaneously after photoexcitation. We show that the transient conductivity spectrum is dominated by two major contributions: response of separated charge carriers and response of coupled polaron pairs.

1. Introduction

Conjugated organic semiconductors are intensively explored for instance due to the envisaged application as the basic active material in inexpensive solar cells.[1,2] While neat polymers are poor solar cell materials due to inefficient dissociation of initially photogenerated excitons,[3] a much greater efficiency is achieved when the polymer is blended with an electron acceptor, giving rise to a so-called bulk heterojunction.[4] Despite numerous improvements in past years, current organic solar cells still suffer from low power conversion efficiency, which hardly reaches ∼5%.[5] Further increase can be achieved by employing a tandem-cell geometry: an overall power conversion efficiency of 6.7% has been recently demonstrated by Kim et al.[6] The ultimate efficiency of solar cells is influenced by basic photoinitiated processes including light harvesting, charge separation, and subsequent charge transport to electrodes.[7] Detailed understanding of these processes is thus essential for development of more efficient materials.

Time-resolved terahertz (THz) spectroscopy is a noncontact method, which can probe instantaneous far-infrared response upon photoexcitation with sub-picosecond temporal resolution.[8] In this method, THz pulses are used to probe the response induced by ultrashort optical excitation pulses. Since the THz pulses are generated and detected coherently, this method yields both the real and imaginary part of transient conductivity spectra. From the spectrum, it is possible to directly infer on the degree of localization of photogenerated charge carriers and thus to distinguish the response of mobile charge carriers from the response of localized excitations like excitons.[9,10]

Blends of polyfluorene copolymers with PCBM are very promising active materials for organic solar cells, with power conversion efficiencies reaching 2.8%.[11] In this paper, we investigate photoinitiated dynamics in a low band gap copolymer poly[2,7-(9,9-dioctyl-fluorene)-alt-5,5-(4′,7′-di-2-thienyl-2′,1′,3-benzo-thiadiazole)] (APFO-3, inset of Figure 1)[12] and in its blends with a soluble fullerene derivative [6,6]-phenyl-C_{61}-butyric acid methyl ester (PCBM[13]) in several weight ratios. We thus complement the recent studies carried out using optical transient absorption spectroscopy[14,15,16] by monitoring the population and mobility of separated charge carriers and bound polaron pairs in short times after photoexcitation.

2. Experimental Methods

The investigated low-band gap polymer APFO-3 consists of two different types of monomer units: a fluorene unit and a low-band gap segment of benzothiadiazole (chemical structure is shown in inset of Figure 1).[12] This copolymer was dissolved in chloroform and blended with PCBM. Samples with PCBM weight fractions c_{PCBM} of 0, 0.50, 0.67, and 0.80 have been prepared. Since samples for the THz measurements should absorb the vast majority of the incident excitation beam in order to exhibit a measurable transient THz response, relatively thick (∼1 μm) films were deposited by drop casting the solution on a 1 mm thick fused silica substrate. Another set of samples was used for optical absorption measurement: these ∼100 nm thick films were deposited by spin-coating on glass substrates.

The THz measurements were carried out using a THz setup similar to that described in ref 17. In brief, a Ti:sapphire optical amplifier delivers a train of 150-fs pulses with 800-nm central wavelength and energy of 1 mJ/pulse. The beam is split into three branches. The first one serves for THz radiation generation by optical rectification in a 1 mm thick ⟨110⟩ ZnTe crystal. The second branch is used for detection of THz pulses by means of electro-optic sampling in another ⟨110⟩ ZnTe crystal. The rest seeds an optical parametric amplifier, which produces 580-nm pulses with energy up to 25 μJ/pulse used for photoexcitation of the sample. Except for fluence-dependence measurements, the excitation fluence was kept at 3×10^{14} photons/cm^2.

Two modes of the THz experiment are employed for the investigations. Information about kinetics is obtained by scanning the pump−probe delay τ, while fixing the point on the THz waveform near the maximum of the photoinduced signal. In the second mode, a few representative pump−probe delays

* To whom correspondence should be addressed. E-mail address: hynek.nemec@chemphys.lu.se.
† Lund University.
‡ Institute for Atomic and Molecular Physics.
§ Linköping University.

10.1021/jp710184r CCC: $40.75
Published on Web 04/03/2008

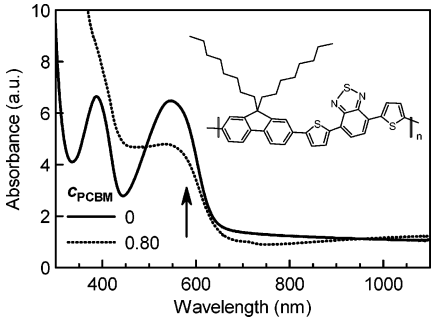

Figure 1. Absorbance spectrum of the neat APFO-3 polymer ($c_{PCBM} = 0$) and of the $c_{PCBM} = 0.80$ blend on the glass substrate. The long-wavelength tail is mainly due to Fresnel losses. The arrow indicates the excitation wavelength. Inset: Chemical structure of the APFO-3 polymer.

τ are chosen, and the corresponding transient transmission spectra $\Delta T(f,\tau)$ are measured. The time-dependent transient conductivity is subsequently calculated from the relation[18,19]

$$\Delta\sigma(f,\tau) = -\alpha\epsilon_0 c(1 + n_s)\frac{\Delta T(f,\tau)}{T(f)} \quad (1)$$

where α is the linear absorption coefficient of the excitation beam, c is the velocity of light in vacuum, ϵ_0 is the permittivity of vacuum, n_s is the refractive index of the substrate, and $T(f)$ is the transmission spectrum of the sample in the ground state. Precisely speaking, $\Delta\sigma$ in eq 1 denotes the transient volume conductivity at the front surface of the sample, which then decays with depth z as $\exp(-\alpha z)$ due to excitation beam absorption. We will rather present our results in terms of conductivity induced by a single photon, which is depth independent and is defined as

$$\Delta\Sigma = \frac{\Delta\sigma}{n_0} = -\frac{1}{F}\epsilon_0 c(1 + n_s)\frac{\Delta T(f,\tau)}{T(f)} \quad (2)$$

where n_0 is the number of excitation events per unit volume and F is the excitation fluence (in photons per m^2). Since $n_0 = \alpha F$, the evaluation of $\Delta\Sigma$ does not require the knowledge of the absorption coefficient α. Equation 2 thus remains valid as long as the transient photoconductivity is proportional to n_0, regardless of possible nonlinear absorption.

Note that during the early stages of the dynamics (pump−probe delays $\lesssim$2 ps), the photoinitiated dynamics involves spectral components mixing with the bandwidth of the probing THz pulse, therefore the simple eqs 1 and 2 cannot be used for evaluation of the transient conductivity for such short times.[18,20]

3. Experimental Results

Examples of optical absorption spectra of the investigated samples are plotted in Figure 1. We observe an onset of strong absorption at ~620 nm, which corresponds to the band gap of the APFO-3 copolymer. Since PCBM molecules start to absorb around 400 nm, we expect that primarily the APFO-3 molecules are excited with the 580-nm excitation beam. Note also that the excitation takes place close to the absorption edge of APFO-3, thus avoiding potential effects associated with hot carrier dynamics.

Kinetic traces are shown in Figure 2a for various blends. In the neat polymer as well as in all blends, the photoinduced signal appears instantaneously during the excitation pulse arrival ($\tau = 0$ ps). For positive pump−probe delays, the signal decays nonexponentially. All traces exhibit an ultrafast component with

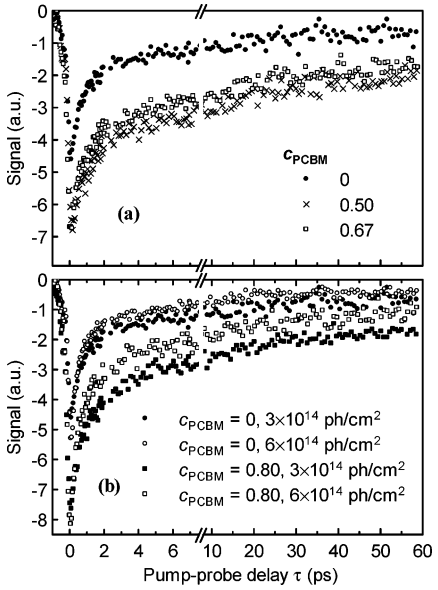

Figure 2. (a) Pump−probe scans in various blends of APFO-3 and PCBM measured with excitation fluence of 3×10^{14} photons/cm^2. The curve for $c_{PCBM} = 0.80$ blend was omitted for graphical clarity since it nearly overlaps the $c_{PCBM} = 0.67$ curve. (b) Normalized kinetic traces for $c_{PCBM} = 0$ and 0.80 blends and for two different excitation fluences.

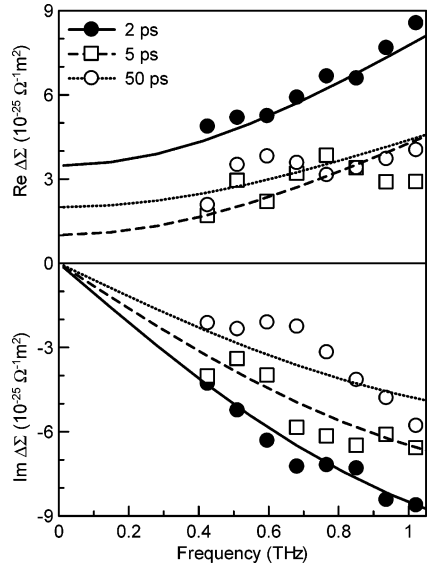

Figure 3. Spectrum of transient conductivity in neat APFO-3 for three representative pump−probe delays. Symbols, measured spectra; lines, fit by eq 3.

a decay time faster than 2 ps, followed by a slower component which stays for more than 1 ns. The amplitude of the signal in the neat polymer is somewhat lower than in the blends.

Figure 2b demonstrates the pump−fluence dependence of the kinetic traces in the neat polymer and in the blend with $c_{PCBM} = 0.80$. In general, increased excitation fluence causes speeding up of the ultrafast component, and a slightly sublinear increase of the amplitude of the slow component of the transient signal.

Transient conductivity evaluated using eq 1 is shown in Figures 3 and 4 for a few representative pump−probe delays. The spectra of all investigated samples have several important features in common. (i) The shape of the spectrum changes only slightly with increasing pump−probe delay, i.e., the kinetics of the underlying physical processes is comparable. (ii) Although the conductivity was not measured at zero frequency, it appears that the real part of the conductivity has a finite nonzero value

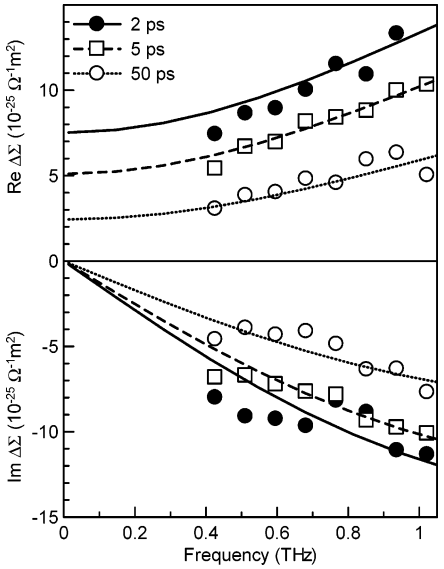

Figure 4. Spectrum of transient conductivity in $c_{PCBM} = 0.80$ blend. Symbols, measured spectra; lines, fit by eq 3.

at 0 THz. This is a signature of charge carriers exhibiting high mobility when probed at least by sub-THz frequencies. (iii) The real part of conductivity increases with frequency, while the imaginary part is negative, and it is a decreasing function. This indicates that the transient conductivity contains another contribution due to much more localized excitations.

4. Model of Charge Carrier Dynamics

We model the measured transient conductivity spectra as a response of two distinct processes

$$\Delta\Sigma(f,\tau) = \Delta\Sigma_0(\tau) + \Delta\Sigma_1(f,\tau) = e_0\xi_0(\tau)\mu_0(\tau) + e_0\xi_1(\tau)\mu_1(\tau)\frac{2\pi i f\theta_1}{2\pi i f\theta_1 - 1} \quad (3)$$

We assign the first term—accounting for the conductivity observed at the lowest frequencies—to the response due to the transport of separated charge carriers. It depends on the quantum efficiency ξ_0 with which these carriers are generated and on their mobility μ_0 (e_0 is the elementary charge). The transport properties are determined by the intrachain transport through polymer chains with finite length[21] as well as to the hopping conduction through a disordered system.[22,23] In either case, the mobility μ_0 is—precisely speaking—frequency dependent: it is very low in a direct current field, and it grows with increasing frequency and saturates well below THz frequencies.[21−23] The THz measurements are sensitive to the value of the saturated mobility only. We will thus call this term as saturated conductivity, and we shall omit its frequency dependence. The lack of data in the unsaturated regime precludes drawing further conclusions about the type of the transport beyond that it is related to intra- and interchain hopping. The second term describes a Debye relaxation process with relaxation time θ_1, which we express in terms of its quantum efficiency ξ_1 and frequency-dependent mobility $\mu_1 2\pi i f\theta_1/(2\pi i f\theta_1 - 1)$. The underlying physical processes will be assigned in the next section.

Very reasonable fits are obtained provided that the relaxation time θ_1 is independent both of the blending ratio and of the pump−probe delay τ. However, we assume that the products $\xi_j\mu_j$ can depend both on the composition of the sample and on the pump−probe delay. As a result, we obtained $\theta_1 = 80$ fs.

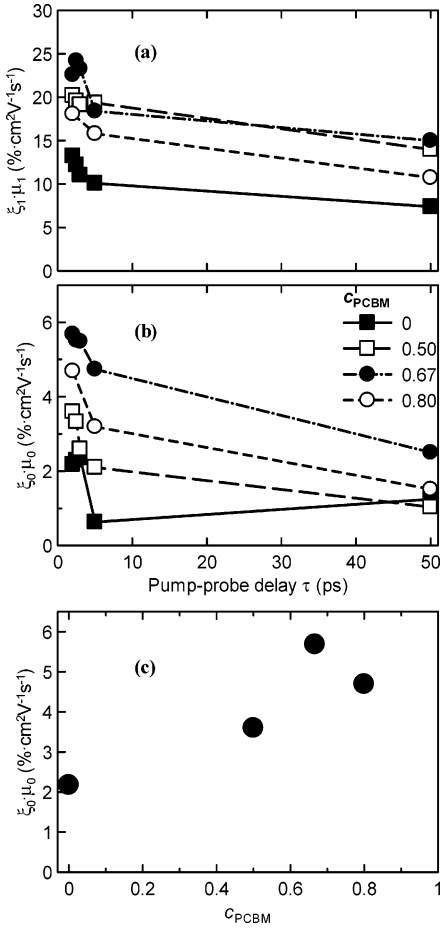

Figure 5. (a) Product of the quantum efficiency of the relaxator term and of the corresponding mobility as a function of pump−probe delay. (b), (c) Product of the quantum efficiency in the saturated conductivity and corresponding mobility as a function of pump−probe delay (b) and as a function of PCBM concentration 2 ps after photoexcitation (c).

The products $\xi_j\mu_j$ are summarized in Figure 5 as a function of pump−probe delay and composition, respectively. Comparison of the results of the fitting model and measured data is shown in Figures 3 and 4.

Note that the experiments allow to determine the quantum efficiency of the charge carrier generation ξ_j and the corresponding mobility μ_j in the form of the product $\xi_j\mu_j$ only: separate evaluation of ξ_j or μ_j would require additional assumptions. These products along with the value of the relaxation time θ_1 thus represent the basic result provided by time-resolved THz spectroscopy in the framework of the model characterized by eq 3.

5. Discussion

5. 1. Neat Polymer. Relaxation Term. It is generally agreed that excitons are the primary product of photoexcitation in neat polymers, with photon-to-exciton conversion quantum efficiency approaching unity at low excitation intensities.[24] The lifetime of excitons in APFO-3 is ∼2 ns, it can be thus regarded as time-independent of the time scales examined in our THz experiments (though the lifetime shortens at high excitation intensities as a result of exciton−exciton annihilation[16]). From the polarizability of excitons of ≤ 0.24 C^2 m^2 J^{-1} provided in ref 25 for a poly(9,9-dioctyl)fluorene, we can estimate their far-infrared response[26] to be at most $\Delta\Sigma_{exciton} \approx -if(1.2 \times 10^{-25}$ Ω^{-1} m^2 THz^{-1}) with a negligible real part. In reality, the

excitonic response will be lower especially due to exciton−exciton annihilation, which decreases the population of excitons. Since the observed imaginary part of conductivity for the shortest pump−probe delays reaches $-9 \times 10^{-25}\ \Omega^{-1}\ m^2$ at 1 THz, it is clear that the response of excitons cannot form a major contribution to the observed conductivity.

According to the kinetic model developed in ref 16, the first excitonic state S_1 can evolve along three channels. First, the exciton can be converted into interchain polaron pairs. Under low excitation fluence, this process is very slow (~5 ns), therefore it cannot contribute to the observed THz spectra. Interchain polaron pairs can be also created as a product of exciton−exciton annihilation; their lifetime is longer than 100 ps. Finally, vibronically excited S_1 excitons can form intrachain polaron pairs with lifetime of 2.4 ps. We thus interpret the decay in the first few picoseconds of the amplitude of relaxation from Figure 5a as a response of intrachain polaron pairs, while the much slower one (tens of picoseconds) represents the response of interchain polaron pairs. The relaxator term in eq 3 can be then assigned to the relaxation of the dipole moment associated with a polaron pair. Considering the fact that the relaxator model is a limiting case of an overdamped oscillator model, the shortness of the relaxation time θ_1 indicates a rather strong binding of the polaron pair.

Saturated Conductivity. As we pointed out in section 4, the saturated conductivity originates from the response of separated charge carriers. Under low excitation fluence, separated charge carriers are predominantly formed as a product of dissociation of S_1 excitons into interchain polaron pairs and their subsequent separation. However, the rate of this process—determined by interchain polaron-pair lifetime of 5 ns—is too slow to create any measurable response during the tens of picoseconds time scale employed in the experiments.

Since we are using high excitation densities ($4.9 \times 10^{19}\ cm^{-3}$), nonlinear phenomena including exciton−exciton annihilation or sequential excitation can act as the precursor for generation of separated charge carriers[27] During exciton−exciton annihilation, one exciton relaxes to its ground state, while its energy is transferred to another exciton that is excited to a higher excitonic state S_n. The S_n exciton subsequently relaxes back to the S_1 state or produces a separated charge state. In the case of the poly(9,9-dioctyl-fluorene), the exciton−exciton annihilation generates an intermediate state not sooner than around 1 ps after photoexcitation at comparable excitation densities.[28] This interpretation is thus inconsistent with the observed instantaneous response.

In the case of sequential excitation, the first photon excites the S_1 state, and the second photon promotes it further to the S_n state, which can then rapidly ionize into separated charges. This means that separated charges are generated during the excitation pulse duration, in agreement with the observed instantaneous response. We have observed a nearly linear excitation−fluence dependence of the measured far-infrared conductivity spectra. This is consistent with the case of high excitation fluence regime, when the ground-state transition saturates, giving thus rise to the S_n population increasing linearly with excitation fluence. Note also that this model was used to explain the far-infrared dynamics in ref 9.

To estimate the density of charge carriers generated by the sequential excitation, we adopt the results obtained by Silva et al.[29] on poly(6,6′,12,12′-tetraoctyl-2,8-indenofluorene) using transient absorption spectroscopy. For the excitation fluence of ~200 $\mu J/cm^2$ used in our experiments, the density of separated charge carriers generated through sequential excitation reaches ~$2.4 \times 10^{18}\ cm^{-3}$, and it decays to ~$1.2 \times 10^{18}\ cm^{-3}$ in 2 ps after photoexcitation (Figures 4 and 2b in ref 29, respectively). Note that for this excitation fluence, the ground-state electronic transition is indeed saturated and the density of separated charge carriers depends on the excitation fluence linearly. From our measured product $\xi_0\mu_0$ (Figure 5b), we can now evaluate the mobility to be $\mu_0 \approx 0.9\ cm^2\ V^{-1}\ s^{-1}$. This mobility is about 4 orders of magnitude higher than that reported in ref 30 on the same polymer. As we have pointed out in section 4, this difference originates from dispersion of conductivity between direct current and sub-THz frequencies, caused by hopping transport and due to limited transport along polymer chains with finite length. On the other hand, the reported mobility is much lower than the intrachain mobility estimated from microwave measurements in ref 21 for ladder-type poly(*p*-phenylene). This indicates that the structure of the APFO-3 chains is more disordered than the structure of ladder-type poly(*p*-phenylene).

A certain fraction of photons can generate separated charge carriers directly.[31] This fraction varies significantly among various polymers and solvents; it can be (within order of magnitude) comparable to the fraction of free charges via two-step photoexcitation. Since these two processes are both scaled linearly by the excitation fluence (in the range employed in our experiments), we have no means to distinguish between them. In any case, we can conclude that the initial mobility of separated charge carriers is of the order of 1 $cm^2\ V^{-1}\ s^{-1}$.

5. 2. Blends. Though the photoconductive properties of blends distinctly differ from those of polymers, the contrast in far-infrared response is much less pronounced. We thus conclude that a non-negligible part of the far-infrared response in blends has a similar origin as in neat polymer. Nevertheless, presence of the PCMB electron acceptor clearly alters the far-infrared response in blends with 0.67 and 0.80 PCBM concentration.

Relaxation Term. The most important localized excitation in blends is a coupled polaron pair with the positive polaron bound to the polymer and the negative polaron residing on the fullerene ball. De et al. have found from transient absorption studies that these pairs are created within 200 fs after photoexcitation and that their lifetime is of the order of tens of picoseconds at low excitation fluence.[14] The dynamics of the amplitude $\xi_1\mu_1$ in Figure 5a is then in agreement with these findings. In the fits, we adopted the assumption that identical relaxation time takes place in the neat polymer as well as in all the blends, since lifting this assumption does not change the fits significantly. A possible change in the relaxation time with composition would not significantly change the transient far-infrared spectrum, but it would rather influence the dependence of the extracted product $\xi_1\mu_1$ on the blending ratio.

Saturated Conductivity. The product of the separated charge carrier quantum efficiency and the mobility of separated charge carriers (Figure 5c) is increased by the addition of PCBM. The increase could be partially explained by an increase of mobility due to *n*-type conductivity of PCBM. However, the nonmonotonous dependence rather suggests that additional separated charge pairs are generated directly upon photoexcitation.[31] The $\xi_0\mu_0$ product peaks for 0.67 concentration of PCBM, reaching a value of about 6%·$cm^2\ V^{-1}\ s^{-1}$. It is interesting to note that charge formation efficiency in solar cells has a flat maximum around a similar concentration, in contrast to, e.g., the short circuit current density.[15]

The tens of picoseconds decay of $\Delta\Sigma_0(\tau)$ attributed to separated charges seems to be surprisingly fast if we keep in mind that 45% of the photogenerated charge carriers reach the electrodes when APFO-3 and PCBM are used in solar cells.[12]

However, under open-circuit condition, the separated charges will have a tendency to migrate to sites with the lowest potential energy and thus become localized. The accompanying decay of the far-infrared response $\Delta\Sigma_0(\tau)$ can then be interpreted as a decrease of mobility of initially photogenerated separated charge carriers. Note that the trapping does not necessarily harm the operation of the solar cells: unless the trapped charge carriers recombines, they can still reach the electrodes, though on a much longer time scale.

5.3. Common Remarks. A similar investigation using time-resolved THz spectroscopy has been conducted on the regioregular poly(3-hexylthiophene) (RR-P3HT) bulk heterojunction by Ai et al.[32] The authors interpret the results in terms of the Drude−Smith model, which has been intended to account for charge carriers that can exhibit long-range transport as well as strong localization.[33] This model nicely fits the THz response, but it cannot simply account for the discrepancy between direct current and THz mobilities. Nevertheless, we can still straightforwardly compare our product $\xi_0\mu_0$ and the product of the quantum efficiency and alternating current mobility given in ref 32: both these quantities characterize the low-THz-frequency spectra and describe the conductivity related to separated charge carriers. For RR-P3HT, this product varies between 190%· cm^2 V^{-1} s^{-1} for the neat polymer and 280% cm^2 V^{-1} s^{-1} for 0.2 concentration of PCBM (2 ps after photoexcitation).[32] It is thus about 50 times higher as compared to APFO-3:PCBM heterojunctions (Figure 5c). This can be explained by the regioregularity of P3HT: well-organized straight polymer chains exhibit mobilities much larger than disordered APFO-3 polymer chains. Note that despite the dramatic difference in the THz conductivity early after photoexcitation, the best solar cells based on APFO-3:PCBM and RR-P3HT:PCBM blends show similar power conversion efficiencies, 2.6 and 5.0%, respectively,[5,34] and close external quantum efficiencies between 450 and 600 nm.[34,36] In other words, we do not observe any correlation between the far-infrared conductivity during the early times after photoexcitation and conversion efficiency of solar cells based on bulk heterojunctions.

A series of measurements of time-resolved far-infrared conductivity have been performed on poly{2-methoxy-5-(2′-ethyl-hexyloxy)-*p*-phenylene-vinylene} (MEH-PPV) by Hendry et al.[9,10,26] In this material, the authors demonstrate that separated charge carriers exist only hundreds of femtoseconds after photoexcitation, and they interpret the corresponding conductivity in terms of intramolecular charge transport along isolated polymer chains limited by torsional disorder and polymerization defects. At longer times, only response of excitons has been observed, with a quantum efficiency reaching 100%. The difference in the transient far-infrared spectra in MEH-PPV and APFO-3 might originate from different excitation conditions (higher excess energy, order of magnitude higher excitation density) as well as from distinct properties of these materials. In particular, the lowest excited state of APFO-3 is of a charge-transfer nature, whereas in MEH-PPV it is a $\pi-\pi^*$ state.[15]

Microwave radiation is another long-wave probe of the transport properties. However, the temporal resolution of time-resolved microwave conductivity is typically worse than 10 ns,[35] implying that completely different processes could be probed. Notably, the major process of creation of separated charge carriers in blends through exciton dissociation into coupled polaron pairs and subsequent charge separation is completed in less than 100 ps.[14] The microwave spectra 10 ns after photoexcitation are thus dominated by the response of these separated charge carriers.[35] Conversely, in our work we examine tens of picoseconds times, when dissociation of coupled polaron pairs only starts: the observed response thus contains also contribution from separated charge carriers formed through different (faster) channels.

6. Conclusion

We have measured the transient far-infrared conductivity spectrum of photoexcited blends of the low band gap polyfluorene polymer APFO-3 and an electron acceptor PCBM. The observed spectrum is dominated by response of separated charges and by response of coupled polaron pairs. We determined the product of the quantum efficiency and mobility of these excitations as a function of time after photoexcitation and blending ratio. We have not found any significant correlation between the far-infrared conductivity in the first picoseconds after photoexcitation and the power conversion efficiency of solar cells based on different polymer:electron acceptor blends. This means that the probed spectral range must be extended in order to characterize the excitations controlling the solar cell power conversion efficiency. A correlation was however found between the picosecond far-infrared conductivity and the charge formation efficiency in APFO-3:PCBM blends.

Acknowledgment. The studies were supported by the Swedish Energy Administration and by the Center of Organic Electronics funded by the Swedish Strategic Research Foundation. H.N. also acknowledges the Swedish Institute for the support through the Guest Scholarship Programme.

References and Notes

(1) Brabec, J. C. *Solar Energy Mater. Solar Cells* **2004**, *83*, 273−292.
(2) Günes, S.; Neugebauer, H.; Sariciftci, N. S. *Chem. Rev.* **2007**, *107*, 1324−1338.
(3) Gulbinas, V.; Zaushitsyn, Y.; Sundström, V.; Hertel, D.; Bässler, H.; Yartsev, A. *Phys. Rev. Lett.* **2002**, *89*, 10 7401.
(4) Yu, G.; Gao, J.; Hummelen, J. C.; Wudl, F.; Heeger, A. J. *Science* **1995**, *270*, 1789−1791.
(5) Reyes-Reyes, M.; Kim, K.; Carroll, D. L. *Appl. Phys. Lett.* **2005**, *87*, 08 3506.
(6) Kim, J. Y.; Lee. K.; Coates, N. E.; Moses, D.; Nguyen, T.-Q.; Dante, M.; Heeger, A. J. *Science* **2007**, *317*, 222−225.
(7) Brédas, J. L.; Beljonne, D.; Coropceanu, V.; Cornil, J. *Chem. Rev.* **2004**, *104*, 4971−5003.
(8) Schmuttenmaer, C. A. *Chem. Rev.* **2004**, *104*, 1759−1779.
(9) Hendry, E.; Schins, J. M.; Candeias, L. P.; Siebbeles, L. D. A.; Bonn, M. *Phys. Rev. Lett.* **2004**, *92*, 19 6601.
(10) Hendry, E.; Koeberg, M.; Schins, J. M.; Siebbeles, L. D. A.; Bonn, M. *Chem. Phys. Lett.* **2006**, *432*, 441−445.
(11) Zhang, F.; Jespersen, K. G.; Björström, C.; Svensson, M.; Andersson, M. R.; Sundström, V.; Magnusson, K.; Moons, E.; Yartsev, A.; Inganäs, O. *Adv. Funct. Mater.* **2006**, *16*, 667−674.
(12) Inganäs, O.; Svensson, M.; Zhang, F.; Gadisa, A.; Persson, N. K.; Wang, X.; Andersson, M. R. *Appl. Phys. A* **2004**, *79*, 31−35.
(13) Hummelen, J. C.; Knight, B. W.; LePeq, F.; Wudl, F.; Yao, J.; Wilkins, C. L. *J. Org. Chem.* **1995**, *60*, 499−503.
(14) De, S.; Pascher, T.; Maiti, M.; Jespersen, K. G.; Kesti, T.; Zhang, F.; Inganäs, O.; Yartsev, A.; Sundström, V. *J. Am. Chem. Soc.* **2007**, *129*, 8466−8472.
(15) Jespersen, K. G.; Beenken, W. J. D.; Zaushitsyn, Y.; Yartsev, A.; Andersson, M.; Pullerits, T.; Sundström, V. *J. Chem. Phys.* **2004**, *121*, 12613−12617.
(16) Westerling, M.; Aarnio, H.; Österbacka, R.; Stubb, H.; King, S. M.; Monkman, A. P.; Andersson, M. R.; Jespersen, K. G.; Kesti, T.; Yartsev, A.; Sundström, V. *Phys. Rev. B* **2007**, *75*, 22 4306.
(17) Beard, M. C.; Turner, G. M.; Schmuttenmaer, C. A. *Phys. Rev. B* **2000**, *62*, 15764−15777.
(18) Nienhuys, H.-K.; Sundström, V. *Phys. Rev. B* **2005**, *71*, 23 5110.
(19) Kužel, P.; Kadlec, F.; Němec, H. *J. Chem. Phys.* **2007**, *127*, 02 4506.
(20) Němec, H.; Kadlec, F.; Kadlec, C.; Kužel, P.; Jungwirth, P. *J. Chem. Phys.* **2005**, *122*, 10 4504.

(21) Prins, P.; Grozema, F. C.; Schins, J. M.; Siebbeles, L. D. A. *Phys. Status Solidi B* **2006**, *243*, 382−386.
(22) Dyre, J. C. *J. Appl. Phys.* **1988**, *64*, 2456−2468.
(23) Ltaief, A.; Bouazizi, A.; Davenas, J.; Alcouffe, P.; Chaâbane, R. B. *Thin Solid Films* **2006**, *511*−512, 498−505.
(24) Scheblykin, I. G.; Yartsev, A.; Pullerits, T.; Gulbinas, V.; Sundström, V. *J. Phys. Chem. B* **2007**, *111*, 6303−6321.
(25) Cadby, A. J.; Lane, P. A.; Mellor, H.; Martin, S. J.; Grell, M.; Giebeler, C.; Bradley, D. D. C.; Wohlgenannt, M.; An, C.; Vardeny, Z. V. *Phys. Rev. B* **2000**, *62*, 15604−15609.
(26) Hendry, E.; Koeberg, M.; Schins, J. M.; Nienhuys, H. K.; Sundström, V.; Siebbeles, L. D. A.; Bonn, M. *Phys. Rev. B* **2005**, *71*, 12 5201.
(27) Stevens, M. A.; Silva, C.; Russell, D. M.; Friend, R. H. *Phys. Rev. B* **2001**, *61*, 16 5213.
(28) Xu, Q.-H.; Moses, D.; Heeger, A. J. *Phys. Rev. B* **2003**, *68*, 17 4303.
(29) Silva, C.; Dhoot, A. S.; Russell, D. M.; Stevens, M. A.; Arias, A. C.; MacKenzie, J. D.; Greenham, N. C.; Friend, R, H.; Setayesh, S.; Müllen, K. *Phys. Rev. B* **2001**, *64*, 12 5211.
(30) Andersson, L. M.; Inganäs, O. *Appl. Phys. Lett.* **2006**, *88*, 08 2103.
(31) Sheng, C.-X.; Tong, M.; Singh, S.; Vardeny, Z. V. *Phys. Rev. B* **2007**, *75*, 08 5206.
(32) Ai, X.; Beard, M. C.; Knutsen, K. P.; Shaheen, S. E.; Rumbles, G.; Ellingson, R. J. *J. Phys. Chem. B* **2006**, *110*, 25462−25471.
(33) Smith, N. V. *Phys. Rev. B* **2001**, *64*, 15 5106.
(34) Gadisa, A.; Zhang, F.; Sharma, D.; Svensson, M.; Andersson, M. R.; Inganäs, O. *Thin Solid Films* **2007**, *515*, 3126−3131.
(35) Savenije, T. J.; Kroeze, J. E.; Wienk, M. M.; Kroon, J. M.; Warman, J. M. *Phys. Rev. B* **2004**, *69*, 15 5205.
(36) Li, G.; Yao, Y.; Yang, H.; Shrotriya, V.; Yang, G.; Yang, Y. *Adv. Funct. Mater.* **2007**, *17*, 1636.